Journal of MATERIALS RESEARCH

Article
DOI:10.1557/s43578-022-00730-y

On the relationships between hardness and the elastic and plastic properties of transversely isotropic power-law hardening materials

T. S. Bhat[1], T. A. Venkatesh[1,a)]

[1] Department of Materials Science and Chemical Engineering, Stony Brook University, New York, NY 11794, USA
[a)] Address all correspondence to this author. e-mail: t.venkatesh@stonybrook.edu

Received: 11 May 2022; accepted: 6 September 2022

Using a combination of dimensional analysis and large deformation finite element simulations of indentations of power-law hardening model materials, a framework for capturing the hardness characteristics of transversely isotropic materials is developed. By considering 4800 combinations of material properties, relationships that predict the hardness of transversely isotropic materials are formulated for both longitudinal and transverse indentations. It is found that hardness tends to be higher for materials with plastic anisotropy than those that exhibit equivalent elastic anisotropy. For perfectly plastic materials, the hardness to the yield stress ratio (R_0) can vary from 2.5 to 3.5, while for materials with strain hardening, R_0 can be as high as 10. A tighter relationship between the hardness and the Tabor's representative stress is observed with the ratio of the hardness to the Tabor's representative stress (R_t) ranging from 2.2 to 4, depending on the elastic and plastic properties and the degree of anisotropy.

Introduction

For nearly 100 years, there has been continued interest in the indentation-based testing of materials in order to assess the hardness and tribological performance of a material and to obtain insights on several other aspects of the mechanical behavior of materials such as their elastic, plastic, fracture, and creep properties. Particularly, in recent times, with improvements in the technology of indentation testing and the expansion of the range materials that are of interest to the engineering community, more efforts have been made to understand several other properties of materials such as electro-mechanical, magneto-mechanical, and shape-memory behavior using the indentation process [e.g., 1–30]. With the ability to span a range of length-scales from the nano-level to the micro-level, the potential for the indentation method to provide fundamental knowledge about the deformation processes and their impact on the mechanical behavior of materials at the nano- and micro-level in small volume structures such as nano-pillars, nano-wires, thin films, coatings, graded materials, and 3-D printed structures has been well recognized as well [e.g., 31–37].

However, due to the complexity associated with the interpretation of the experimentally observed indentation response of materials and correlating it with the fundamental mechanical properties (i.e., elastic, plastic, strain-hardening, and hardness properties) of the indented materials, much of the prior studies have focused on *isotropic* materials [e.g., 13, 27]. As there are many naturally occurring materials and engineered bulk and thin film materials that exhibit varying degrees of *anisotropy* in both their elastic and plastic domains [e.g., 38–44], there is a strong motivation for understanding the indentation behavior and hardness response of such anisotropic materials as well.

For example, zirconium alloys used as cladding material for fuel rods in nuclear reactors exhibit texture and direction-dependent plastic and hardness properties in the as-fabricated state. Furthermore, with non-uniform exposure to radiation, the irradiated zirconium alloys also exhibit anisotropy in their plastic and hardness properties as well [38]. Nickel–aluminum coatings deposited by various spray techniques such as air plasma spray, high-velocity oxy-fuel, and cold spray have also been found to exhibit anisotropic plastic yield behavior in the in-plane and out-of-plane directions [39]. Nanostructured silver

thin films obtained by electrodeposition methods also display anisotropy in their yield strengths [40]. Rods of SiC whisker-reinforced aluminum alloy A6061, upon drawing and extrusion also demonstrate anisotropy in their plastic properties [41]. Other biomaterials and naturally occurring materials such as cortical bone [42], tooth enamel [43], and wood [44] have also been investigated for their anisotropic characteristics as well. A partial list of engineering materials which exhibit transverse isotropy is presented in Table 1.

Recognizing the importance of anisotropic materials, several studies have analyzed the indentation behavior of anisotropic materials under specific conditions as described below. Vlassak et al. considered the case of *elastically* anisotropic materials and developed an approximate solution for the conical indentation and the effective indentation moduli of such materials [48]. Gao and Pharr developed a method for estimating the elastic moduli of *elastically* anisotropic solids under normal and tangential loading conditions [49]. Jin investigated the indentation behavior of transversely isotropic *elastic* materials under frictionless adhesive contact conditions and demonstrated that the functional forms that capture the indentation responses were similar to those obtained for the indentation of isotropic materials [50]. In another study, also on transversely isotropic *elastic* materials, Borodich et al. determined dimensionless relationships for the indentation force, displacements, and contact radii for frictionless adhesive contacts as well [51]. Li et al. considered the case of *elastically* anisotropic thin films on substrates and obtained insights on the effects of the film thickness on the effective modulus of the thin film on the substrate system [52]. Wang et al. focused on the case of transversely isotropic materials with *plastic* anisotropy and demonstrated that reasonably accurate predictions of the material properties can be obtained using the inverse analysis from the indentation force–depth relationship and pile-up information around the indent obtained from single sharp indentation [53]. Wu et al. developed an inverse analysis for determining the plastic properties of *plastically* anisotropic materials by considering the residual indentation imprints obtained from spherical indentation [54]. Nakamura and Gu developed a dual-indentation method (i.e., a combination of spherical and sharp (Berkovich) indentations) to assess the elastic and plastic properties of transversely isotropic thermally sprayed coating materials [55]. They found that ratios of the elastic moduli and yield strengths in the longitudinal and transverse directions could be determined more robustly compared to the absolute values of the elastic moduli and the yield strengths. Yonezu et al. used dimensional analysis, finite element analysis, and representative strain concept to develop a relationship between the spherical indentation response and the plastic anisotropy of indented materials [56]. Bhat and Venkatesh analyzed the indentation behavior of transversely isotropic materials that exhibit *elastic and plastic* anisotropy, and developed a framework based on dual-sharp and triple-sharp indentation methods, to connect the elastic and plastic properties of transversely isotropic materials, with their indentation responses, through the indentation forward and reverse algorithms [45]. Fan and Rho developed three-dimensional finite element models to assess the effects of *elastic and plastic* anisotropy on the indentation response of cortical bone and demonstrated that the indentation modulus is influenced by anisotropy [42].

However, a comprehensive understanding of the hardness characteristics of transversely isotropic materials and their relationships to their elastic and plastic properties is currently lacking. Hence, the objectives of the present study are as follows:

1. To invoke a combination of dimensional analysis and finite element modeling to develop a framework for predicting the hardness of transversely isotropic materials from a knowledge of the elastic and plastic properties of the indented materials.
2. To formulate a methodology for predicting the hardness of transversely isotropic materials from a knowledge of the indentation force–depth response of the indented materials without the need for explicitly measuring the indentation area of contact.
3. To develop an understanding of the dependence of the hardness of transversely isotropic materials on their elastic and plastic properties.
4. To identify relationships between the hardness of transversely isotropic materials and the Tabor's representative stress and the yield stress.
5. To validate the predictions for the hardness of transversely isotropic materials obtained from the indentation simulations with experimental results for select engineering materials.

Background on transversely isotropic materials and indentation hardness

Transversely isotropic materials

The elastic properties of a transversely isotropic material can be defined with the help of five independent constants namely E_L, E_T, ν_T, ν_{TL}, and G_L or alternatively E_0, E_L/E_T, ν_T, ν_{TL}, and G_L, where E is the elastic modulus, G is the shear modulus, ν_T and ν_{TL} are the in-plane and out-of-plane Poisson's ratios, the subscript 'L' indicates the out-of-plane longitudinal direction, 'T' indicates the in-plane transverse direction, and E_0 is the average Young's modulus—$(E_L + E_T)/2$ (Fig. 1). The plastic properties can also be defined with the help of five independent constants namely σ_L, σ_T, τ_L, τ_T (which are the respective yield stresses in the longitudinal and transverse directions, e.g., ν_T is the normal yield stress and ν_T is the shear yield stress in the

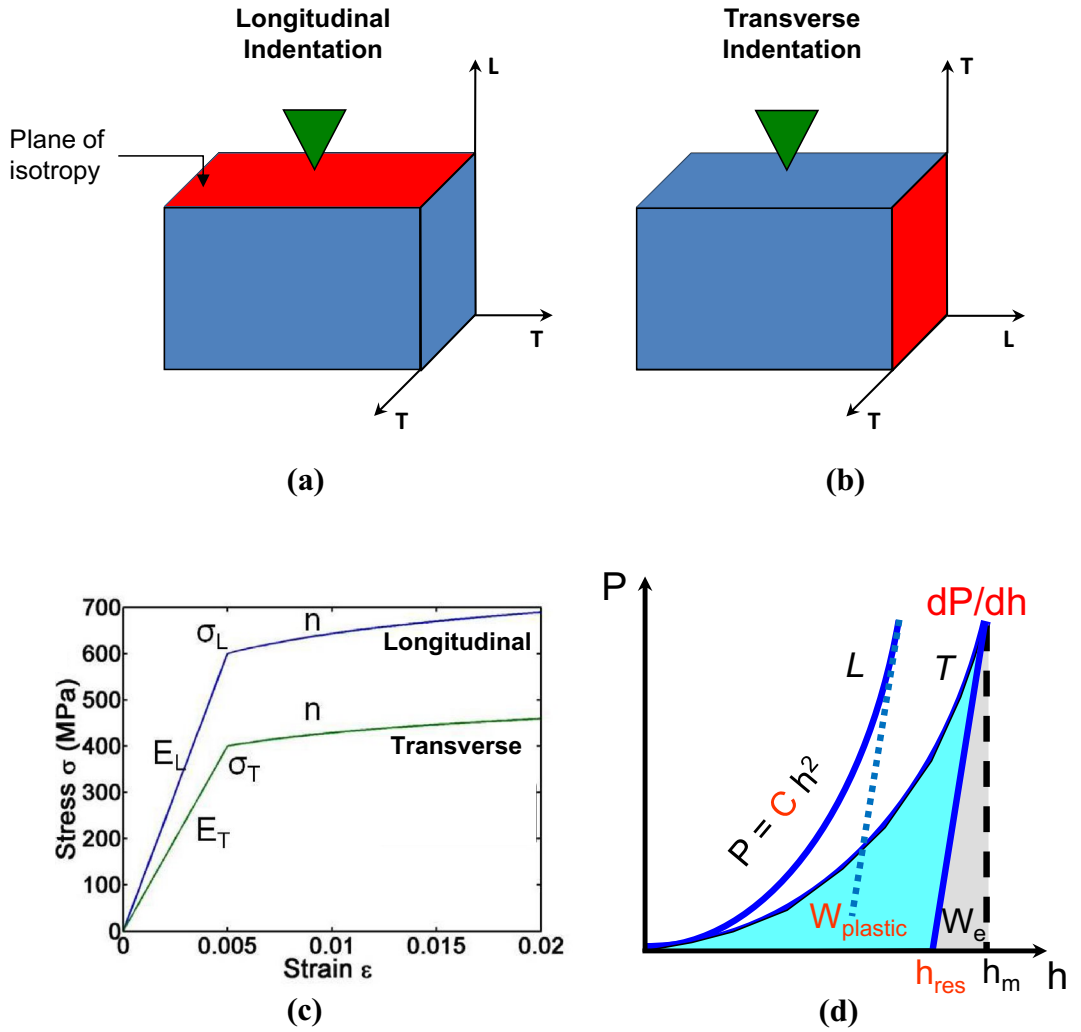

Figure 1: Schematic illustrating (a) longitudinal indentation and (b) transverse indentation of (c) a transversely isotropic material which has different elastic moduli and yield strengths along the transverse and longitudinal directions and (d) the typical load–depth Indentation response of such materials under longitudinal (*L*) and transverse (*T*) indentations.

transverse direction) and n is the strain-hardening exponent. Thus, a total of 10 independent constants are needed for capturing the elastic and plastic properties of transversely isotropic materials (that exhibit similar strain-hardening characteristics (with strain-hardening exponent n) in the in-plane and out-of-plane directions).

However, the inverse indentation analysis for identifying all the 10 material constants, in the most general case of a transversely isotropic material that exhibits a wide variety of combinations of elastic and plastic properties in the in-plane and out-of-plane directions, is very complicated. So, for transversely isotropic materials that exhibit moderate levels of anisotropy in the elastic and plastic properties in the in-plane and out-of-plane directions, the number of material constants required to describe the elastic and plastic properties of transversely isotropic materials can be reasonably reduced from 10 to 5 [Fig. 1(c)], following the approach suggested by Nakamura and Gu [55] as summarized below:

$$\nu_T = \nu_{TL} = 0.3 \tag{1}$$

$$G_L = \frac{(E_L + E_T)}{4(1 + \nu_{TL})} \tag{2}$$

$$\tau_T = \frac{\sigma_0}{\sqrt{3}} \text{ and } \tau_L = \frac{\sigma_0}{\sqrt{3}}\sqrt{\frac{\sigma_L}{\sigma_T}}, \tag{3}$$

where σ_0 is the average yield stress $(\sigma_L + \sigma_T)/2$. The approximation of ν_T and ν_{TL} as 0.3 is reasonable as the Poisson's ratios of most metal and alloys are close to this value. The out-of-plane shear modulus – G_L is also approximated in a manner similar to the definition of the in-plane shear modulus – G_T. Finally, the shear yield stresses in the longitudinal and transverse directions

are approximated in a manner similar to the von Mises yield criterion for isotropic materials.

As transversely isotropic materials have physical properties symmetric about an axis normal to a plane of isotropy, two classes of indentations can be identified [Fig. 1(a), (b)].

(i) Longitudinal indentations, where the indentations are perpendicular to the plane of isotropy; and
(ii) Transverse indentations, where the indentations are parallel to the plane of isotropy.

Indentation hardness

Instrumented indentation involves indenting a substrate material with a flat, sharp, or spherical indenter and observing the corresponding force (P)—depth (h) relationship during the loading and the unloading cycle [Fig. 1(d)]. The indentation hardness (H) of a material is defined as the ratio of load to the projected area of contact.

$$H = \frac{P_m}{A_m}, \tag{4}$$

where A_m is the true projected area of contact at maximum load P_m. The pertinent relationships observed in the force–depth signatures for indentations with a sharp indenter are as follows:

$$P = Ch^2 \tag{5}$$

$$S_m = \left(\frac{dP_u}{dh}\right)\Big|_{h_m} \tag{6}$$

$$R_W = \frac{W_P}{W_T}, \tag{7}$$

where C is the loading curvature for a power-law hardening material, S_m is the slope of the unloading curve at maximum depth of indentation (h_m), P_u is the unloading force, and R_w is the plastic work ratio. The area under the loading curve is the total work done (W_T) and the area under the unloading curve (W_e) represents the recovered elastic work. The plastic work done in the indentation process is given as $W_p = W_T - W_e$.

In general, the P–h response and the area of contact (i.e., the true projected area of contact after accounting for pile-up or sink-in) of a transversely isotropic material (e.g., with $\sigma_L/\sigma_T = 2$; $\sigma_L = 0.28$ GPa and $\sigma_T = 0.14$ GPa) varies considerably from its isotropic counterpart for which the elastic and plastic properties are obtained as a simple average of the properties of the transversely isotropic material (e.g., $\sigma_0 = 0.21$ GPa) (Fig. 2). It can be observed in Fig. 2 that the indentation imprints for transverse indentation show varying degrees of pile-up/sink-in owing to the lack of symmetry of material properties in the plane that is normal to the indentation direction. The projected area of contact in this case has the shape of an ellipse and its magnitude—A_m is also calculated as the area of this ellipse. Overall, the indentation hardness of transversely isotropic materials is expected to depend on the direction of indentation with respect to the plane of isotropy.

Results and discussion

In the present study, two approaches to predict the hardness of transversely isotropic materials have been identified.

Hardness prediction from known material properties

In the first approach, the hardness of the transversely isotropic materials is predicted from known elastic and plastic properties of the indented substrate materials for longitudinal and transverse indentations. For both classes of indentation, the process involves two main steps:

i. Determining the material group within which the material under consideration is bounded.
ii. Applying the corresponding dimensionless functions to obtain the values of the contact area and the indentation hardness for the two indenter orientations.

The dimensionless functions presented in the Methods and Appendix sections were validated by testing them on the 120 materials that were chosen initially to create the database as well as 10 other materials with properties that are bounded within the database. The values for the contact areas and the indentation hardness obtained through the relationships identified were then compared to the corresponding true values obtained from finite element modeling. An excellent match between the two was observed, thus proving the validity of the relationship. Figures 3(a) and (b) provide a comparison of the actual values of the indentation hardness obtained from finite element analysis with that predicted by the dimensionless functions formulated in this study.

Hardness prediction from known indentation response

In the second approach, the hardness of the transversely isotropic materials is predicted from the indentation force–depth characteristics of the indented material. In this method, the inverse analysis presented in an earlier study [45] is first invoked to determine the elastic and plastic properties of the transversely isotropic indented materials from the measured indentation response. Subsequently, the hardness and the area of contact between the indenter and substrate are determined in a manner similar to that described in "Hardness prediction from known material properties" section. Thus, from

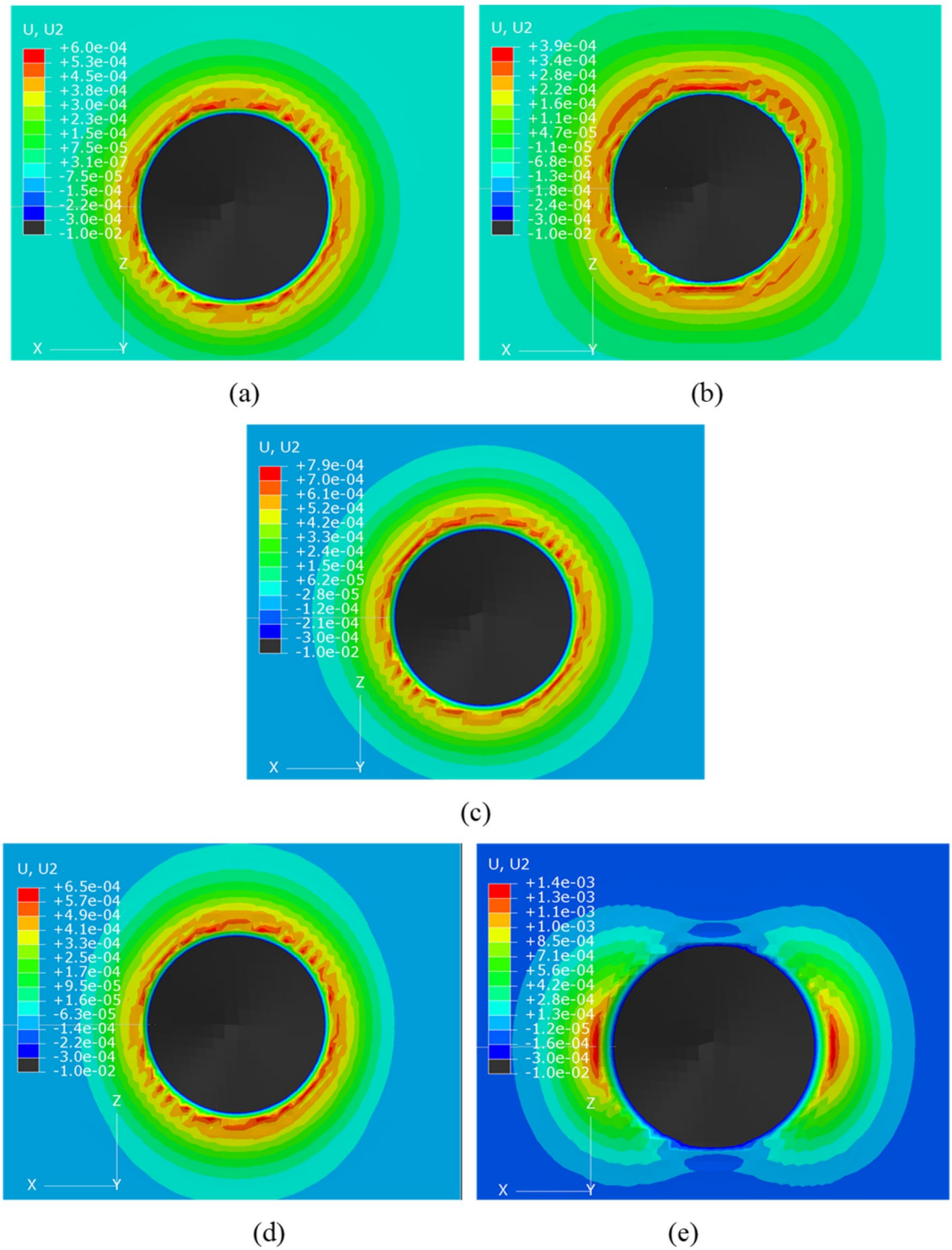

Figure 2: A comparison of the vertical displacement contours displaying the pile-up/sink-in for materials with different degrees of anisotropy: (a) material with elastic anisotropy indented in the longitudinal direction; (b) material with plastic anisotropy indented in the longitudinal direction; (c) isotropic material; (d) material with elastic anisotropy indented in the transverse direction; and (e) material with plastic anisotropy indented in the transverse direction.

the known indentation response of a transversely isotropic material, the hardness of the material is then predicted without the need to actually measure the true area of contact. This is important because there is always some uncertainty as to whether the residual contact area (that is typically measured in a hardness test) represents the true area of contact under

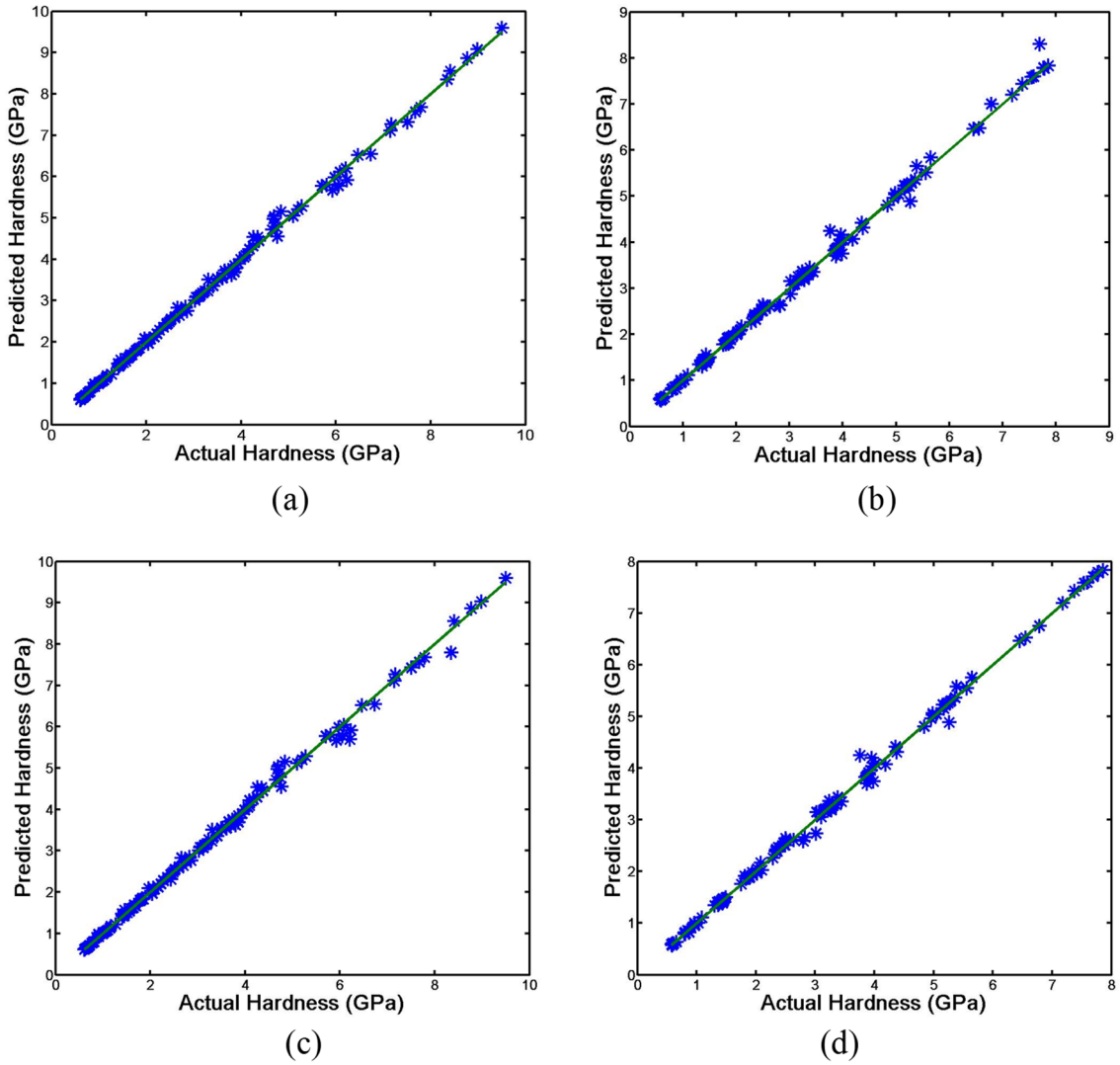

Figure 3: A comparison of the true hardness and that predicted by the model developed in the present study from known elastic and plastic properties, for 130 materials, for (a) indentations perpendicular to the plane of isotropy; and (b) indentations parallel to the plane of isotropy. A comparison of the true hardness and that predicted by the model developed in the present study from known indentation response characteristics for (c) indentations perpendicular to the plane of isotropy; and (d) indentations parallel to the plane of isotropy.

maximum indentation load as the indented material could exhibit pile-up or sink-in upon unloading, resulting in the residual contact area being different from the true contact area. The accuracy of the hardness predictions, as suggested in this method, depends on the accuracy of the reverse analysis used to predict the elastic and plastic properties, which has been demonstrated to be very good in the earlier study [45]. Figure 3(c) and (d) shows that the actual hardness values obtained from finite element analysis compare very well with that obtained through the reverse analysis using dimensionless functions that were identified in this study.

Comparison of hardness obtained from Berkovich and equivalent conical indentations

Within the context of indentation of isotropic materials, it is well recognized that the indentation with a conical indenter with a half-apex angle of 70.3° is equivalent to the indentation with a Berkovich indenter [21]. This equivalence is useful as the finite element simulations of indentations with conical sharp indenters are computationally less expensive. In order to ascertain whether a similar equivalence can be established for the indentation of transversely isotropic materials, three-dimensional finite element simulations were conducted to

compare the indentation hardness obtained from the indentations with a Berkovich indenter and the equivalent conical indenter with a half-apex angle of 70.3°, for both longitudinal and transverse indentations. In order to capture a wide range of indentation scenarios, materials representing lower and higher bounds in the elastic and plastic properties, i.e., elastic moduli, yield strengths, strain-hardening exponents, and elastic and plastic anisotropy, were chosen for the analysis. As illustrated in Table SI, there is very good agreement between the indentation hardness observed in the Berkovich indentations and the equivalent conical indentations. (The maximum difference in the hardness obtained from the conical and Berkovich indentations was observed to be less than 6%.)

Discussion

The traditional method of hardness characterization involves the application of a prescribed indentation load and the measurement of the residual imprint left behind upon complete unloading. As the residual imprint left behind after indentation is primarily due to the plastic deformation of the indented material, initial attempts were focused on understanding the connections between the plastic deformation behavior (i.e., the yield strength) and the hardness of the substrate. For those materials that do not exhibit significant strain hardening, the relationship $H \approx 3\ \sigma_y$ has been widely used. However, through a detailed analysis of the indentation hardness of a large set of isotropic materials, it has been demonstrated that, in general, the hardness of a material is influenced by a combination of its elastic and plastic properties (i.e., the elastic modulus, yield strength, and the strain-hardening characteristics) and the ratio of hardness to the yield strength could vary widely from 2 to 20 (i.e., $H \approx [2–20]\ \sigma_y$) [30]. Thus, the interpretation that the yield strength of an indented material is about a third of its hardness is, in general, not accurate.

For materials that exhibit strain hardening, the relationship $H \approx 3\ \sigma_r$, has also been widely used, where σ_r is a representative stress that corresponds to the Tabor' strain (which, for the case of indentations with a conical indenter with a half-apex angle of 70.3° is about 8%) [57]. A more detailed study has indicated that indeed a tighter connection between the hardness and the plastic deformation characteristics of material can be found by relating the hardness to the representative stress (i.e., $H \approx [2.1–2.8]\ \sigma_r$) for isotropic materials [30].

As the present study has identified functional relationships between the indentation hardness characteristics of transversely isotropic materials and the elastic and plastic properties of the indented materials, there is a natural opportunity to (i) discern the relative influence of the elastic and plastic properties and the level of anisotropy on the effective hardness characteristics; and (ii) assess the possibility of identifying simple relationships between the yield stress or the representative stress and the hardness, in the more complex case of transversely isotropic materials.

The inferences drawn in the present study are predicated upon two important aspects of the present study—one pertaining to the plastic behavior of the indented material and the second pertaining to the depth of indentation. In the finite element analysis conducted in this study, the plastic behavior of the indented materials is modeled as following a power law, which has been widely used before and shown to capture the strain-hardening characteristics of many metals and alloys, reasonably well. Furthermore, the indentations are considered to be deep enough such that potential indentation size effects from shallow indentations are not considered.

Variation of hardness with elastic and plastic anisotropy

Upon validating the accuracy of the dimensionless relationships that capture the indentation hardness of transversely isotropic materials as a function of the materials' elastic and plastic properties with finite element simulations of 130 materials, over 4800 combinations of materials (that are bounded within the overall property domain considered in this study) are invoked to assess carefully the variation of hardness of transversely isotropic materials with the elastic and plastic properties of transversely isotropic materials, using the dimensionless relationships.

The general trends in the variation of hardness of a large group of transversely isotropic materials with elastic anisotropy and plastic anisotropy, (for materials with a constant strain-hardening exponent, e.g., $n = 0.3$), are presented as three-dimensional maps in Fig. 4(a) (for longitudinal indentation) and in Fig. 4(b) (for transverse indentation). As a reference, the variation of hardness for the corresponding isotropic materials is also presented in Fig. 4(a) and (b). By taking a two-dimensional slice that corresponds to, for example, $E_0/\sigma_0 = 160$ in Fig. 4(a), the actual variation of longitudinal hardness for a smaller set of materials (for which $E_0/\sigma_0 = 160$) with yield strength, is visualized as presented in Fig. 4(c). Similarly, the variation of longitudinal hardness with yield strength for the set of materials for which $E_0/\sigma_0 = 220$ is presented in Fig. 4(d). A more detailed perspective of the variation of hardness for a particular material (e.g., with elastic modulus of 150 GPa, yield stress of 0.875 GPa and strain-hardening exponent of 0 or 0.3) as a function of the degree of elastic and plastic anisotropy is presented in Fig. 5. In Fig. 5(a) and (b), the hardness variation for longitudinal indentation of materials with $n = 0$ and $n = 0.3$, respectively, are presented, while in Fig. 5(c) and (d), the hardness variation for transverse indentation of materials with $n = 0$ and $n = 0.3$, respectively, are presented. The observed dependence of hardness of transversely isotropic materials on their elastic moduli,

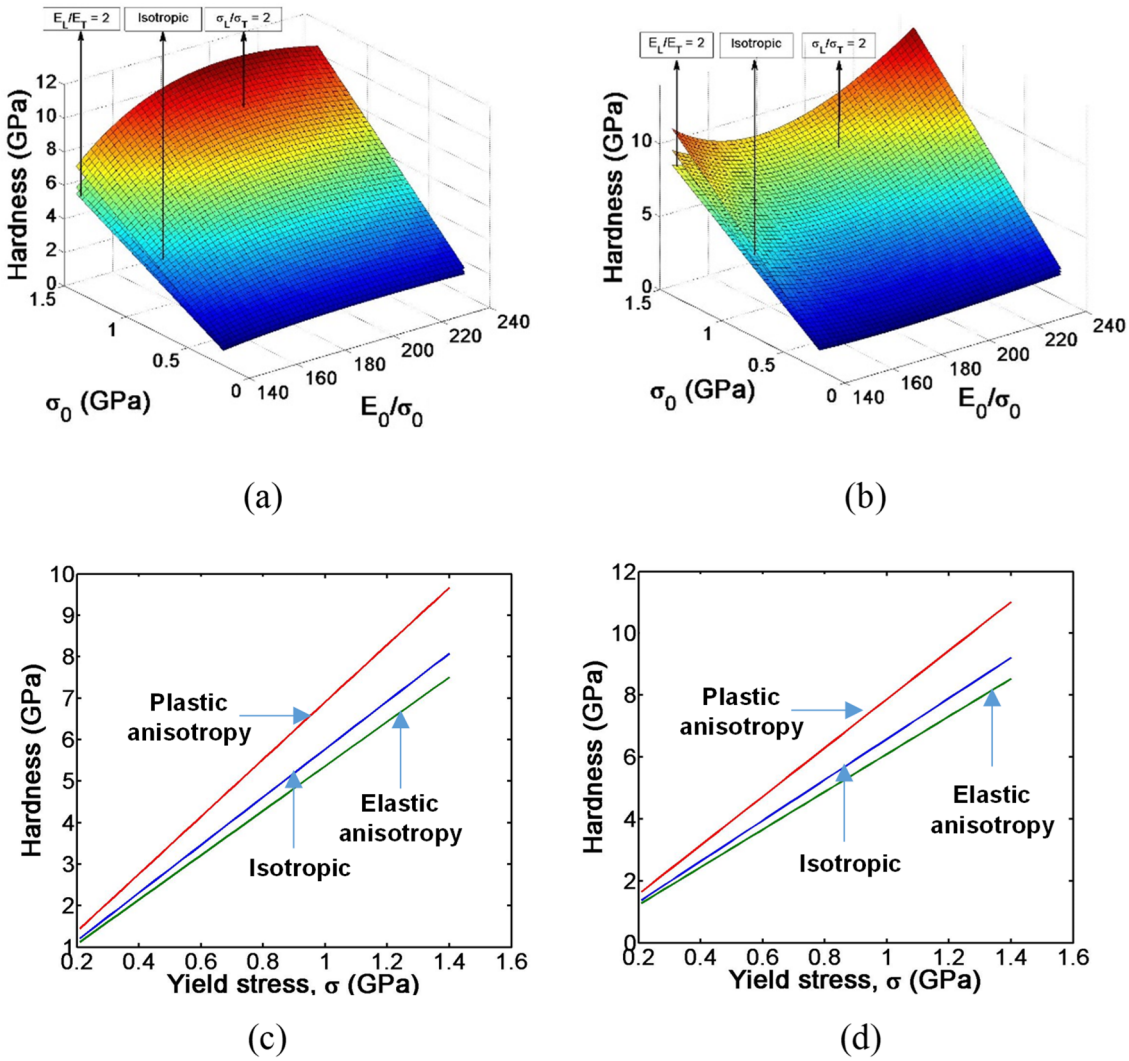

Figure 4: Hardness maps of isotropic materials and materials with elastic and plastic anisotropy (with $n = 0.3$) for (a) longitudinal indentations and (b) transverse indentations. Variation of longitudinal indentation hardness with average yield stress for (c) materials with $E_0/\sigma_0 = 160$ and $n = 0.3$ and (d) for materials $E_0/\sigma_0 = 220$ and $n = 0.3$.

yield strengths, strain-hardening exponents, and the degree of elastic and plastic anisotropy are discussed below.

As has been observed in the case of isotropic materials, the hardness of transversely isotropic materials increases with an increase in the average elastic modulus, the average yield stress, and the strain-hardening exponent (Fig. 4). Due to the dependence of the hardness on both the elastic and plastic properties, it can be expected that some combination of materials which have low stiffness and high yield strengths may exhibit hardness values that are similar to materials with high stiffness and low yield strengths. Indeed, the present analysis of transversely isotropic materials demonstrates that hardness is not a unique material characteristic with multiple materials with different combinations of elastic and plastic properties shown to exhibit identical hardness values.

As transversely isotropic materials could exhibit varying degrees of anisotropy in their elastic and plastic properties, a pertinent question may be posed with regards to the relative influence of the extent of anisotropy, in each of the elastic and plastic domains, on the effective hardness. The present study demonstrates that the hardness of a transversely isotropic material is higher if the material exhibits a certain level of plastic anisotropy (*e.g.*, $E_L/E_T = 1$ and $\boldsymbol{\sigma_L/\sigma_T = 2}$) when compared to a material which exhibits the same level of elastic anisotropy (e.g., $\boldsymbol{E_L/E_T = 2}$ and $\sigma_L/\sigma_T = 1$), when both these materials have the same average elastic modulus and yield strengths. Furthermore, the magnitude of change observed in the hardness due to a certain level of change (e.g., 25%) in the plastic anisotropy is higher than that observed due to the same level of change (i.e., 25%) in elastic anisotropy (Fig. 5). These observations indicate

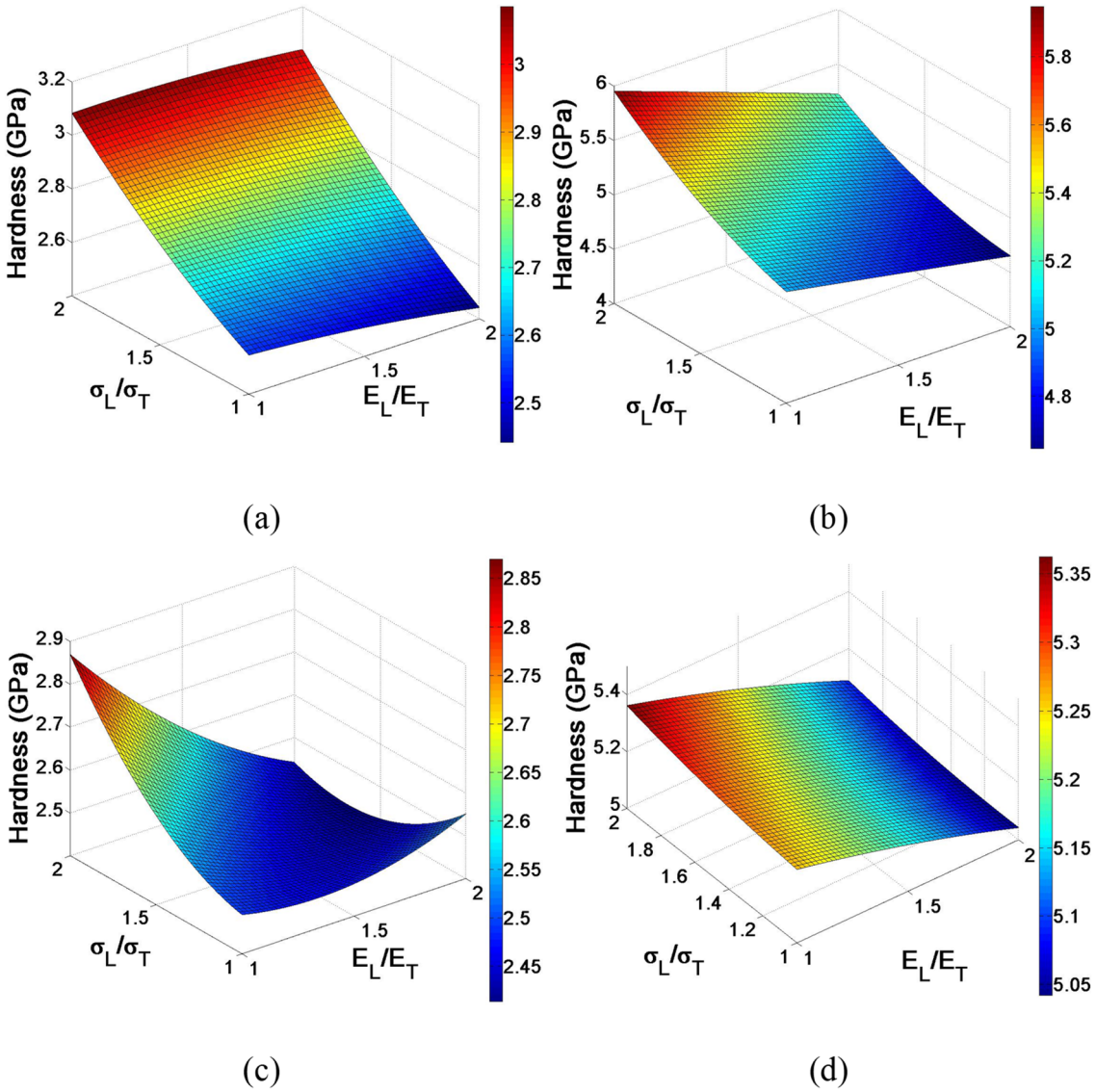

Figure 5: Variation of indentation hardness with varying degree of elastic and plastic transverse isotropy for a material with average yield stress of 0.875 GPa and average elastic modulus of 150 GPa for: (a) longitudinal indentation with no strain hardening; (b) longitudinal indentation of a material with strain-hardening coefficient $n = 0.3$; (c) transverse indentation of a material with no strain hardening; and (d) transverse indentation of a material with strain-hardening coefficient $n = 0.3$.

that although the elastic modulus has an influence on the effective hardness, the effect of the plastic properties is much more dominant. (For example, the increase in the longitudinal yield strength by a factor of 2 has a greater impact on the hardness than the increase in the longitudinal elastic modulus by a factor of 2, while all other material parameters remain unchanged.)

When compared to materials that have low strain-hardening characteristics, the hardness of materials that have higher strain-hardening exhibits a greater level of sensitivity to the anisotropy in the elastic and plastic properties. This effect can be explained by the fact that the materials with higher strain-hardening have a higher upper bound for the flow stress which results in reduced plastic deformation around the indent leading to a reduced contact area (for a fixed indentation load), thus increasing the indentation hardness.

Even though the state-of-stress under the indenter is multiaxial, the indentation hardness is influenced to a greater extent by the effective plastic properties of the material in the loading direction of the indenter. Overall, a variation of up to 25% may be expected in the indentation hardness of transversely isotropic materials obtained in the in-plane and out-of-plane directions, for the range of materials considered in the present study.

Relationship of hardness with yield stress and representative stress

In order to investigate the relationships between the hardness and the plastic deformation behavior (i.e., the yield strength and the characteristic stress) in transversely isotropic materials, the ratio of hardness to the average yield stress (i.e., $R_o = H/\sigma_o$) and ratio of the hardness to the average representative stress (i.e., $R_t = H/\sigma_r$) for materials with elastic anisotropy and plastic anisotropy are studied. The average Tabor representative stress was calculated as the average of the longitudinal and transverse stresses at 8% strain.

As transversely isotropic materials have two values each for the yield stress and the representative stress that correspond to the longitudinal and transverse directions, a simple arithmetic average of these stresses are used in this analysis to identify trends in the dependence of the indentation hardness with yield stress and representative stress. Whether this simple arithmetic average or if some other combination of yield and representative stresses will have a more fundamental significance for understanding the hardness of transversely isotropic materials needs to be assessed in a future study.

Figure 6 presents contour plots for the variation of the ratio of the hardness to the average yield stress (R_0) for longitudinal [Fig. 6(a), (b)] and transverse indentations [Fig. 6(d), (e)], for materials exhibiting elastic anisotropy [Fig. 6(a), (d)] and plastic anisotropy (Fig. 6(b), (e)). As a reference, the variation of R_o in isotropic materials is presented in Fig. 6(c). It is evident that when a wide range of materials with lower and higher levels of strain-hardening are considered, the ratio of hardness to the average yield stress (R_0) can vary from 2.5 to 3.5 for relatively lower strain-hardening materials while the ratio R_0 can be as high as 10 for materials with higher strain-hardening.

Figure 7 presents contour plots for the variation of the ratio of the hardness to average Tabor's representative stress (R_t) for longitudinal [Fig. 7(a), (b)] and transverse indentations [Fig. 7(d), (e)], for materials exhibiting elastic anisotropy [Fig. 7(a, (d)] and plastic anisotropy (Fig. 7b, e). As a reference, the variation of R_t in isotropic materials is presented in Fig. 7(c). It is evident that unlike in the case of the variation of the ratio of hardness to the average yield stress (R_0), the ratio of the hardness to the average representative stress (R_t) provides a relatively tighter bound with the values ranging from 2.2 to 4 for the set of materials considered in the present study.

Overall, this study demonstrates that the hardness of an important class of engineering materials that exhibit transverse isotropy can be predicted well from the knowledge of their elastic and plastic properties. The trends that are observed in the variations of hardness with yield stress and representative stress for transversely isotropic materials are similar to those observed in the case of isotropic materials in that there is a relatively tighter relationship for the hardness with the Tabor's representative stress than the yield strength of the material. However, while the relationship to the Tabor's representative stress is tighter, it is important to note that the hardness of a transversely isotropic material does not correspond to a (universal) constant multiple of the Tabor's representative stress, in a general sense. Hence, caution should be exercised in using hardness as an exclusive predictor of the plastic properties of the indented materials as hardness is influenced by the elastic properties of the indented materials as well.

Comparison of the model predictions of hardness with experimental results for select engineering materials

The model predictions for the hardness of a several materials that exhibit elastic and plastic anisotropy such as tool steel, iron castings, titanium, titanium alloy, aluminum alloy, zirconium, and beryllium-copper alloy are compared to experiments (Table 1, Fig. 8). Where necessary, the Vickers, Brinell, or Rockwell hardness values that have been reported have been converted to the equivalent material hardness (in the units of pressure). It is observed that those materials that exhibit higher yield strengths and higher levels of plastic anisotropy exhibit higher hardness, as expected from the model predictions. Overall, there is a reasonable agreement between the model predictions and experimental observations.

Conclusions

Much of the prior studies in the field of hardness have focused on developing an understanding of the hardness characteristics of isotropic materials. However, several engineering materials in the bulk and thin film form exhibit varying degrees of elastic and plastic anisotropy, and a comprehensive understanding of the hardness behavior of such transversely isotropic materials is not yet available. The present study was focused on developing a framework for predicting and understanding the hardness characteristics of transversely isotropic materials. The principal conclusions from the present study are given below.

(i) Using a combination of finite element modeling and dimensional analysis, explicit functional forms that capture the relationship between the indentation hardness of transversely isotropic materials and their elastic and plastic properties have been identified.
(ii) In general, hardness of transversely isotropic materials increases with an increase in the average elastic modu-

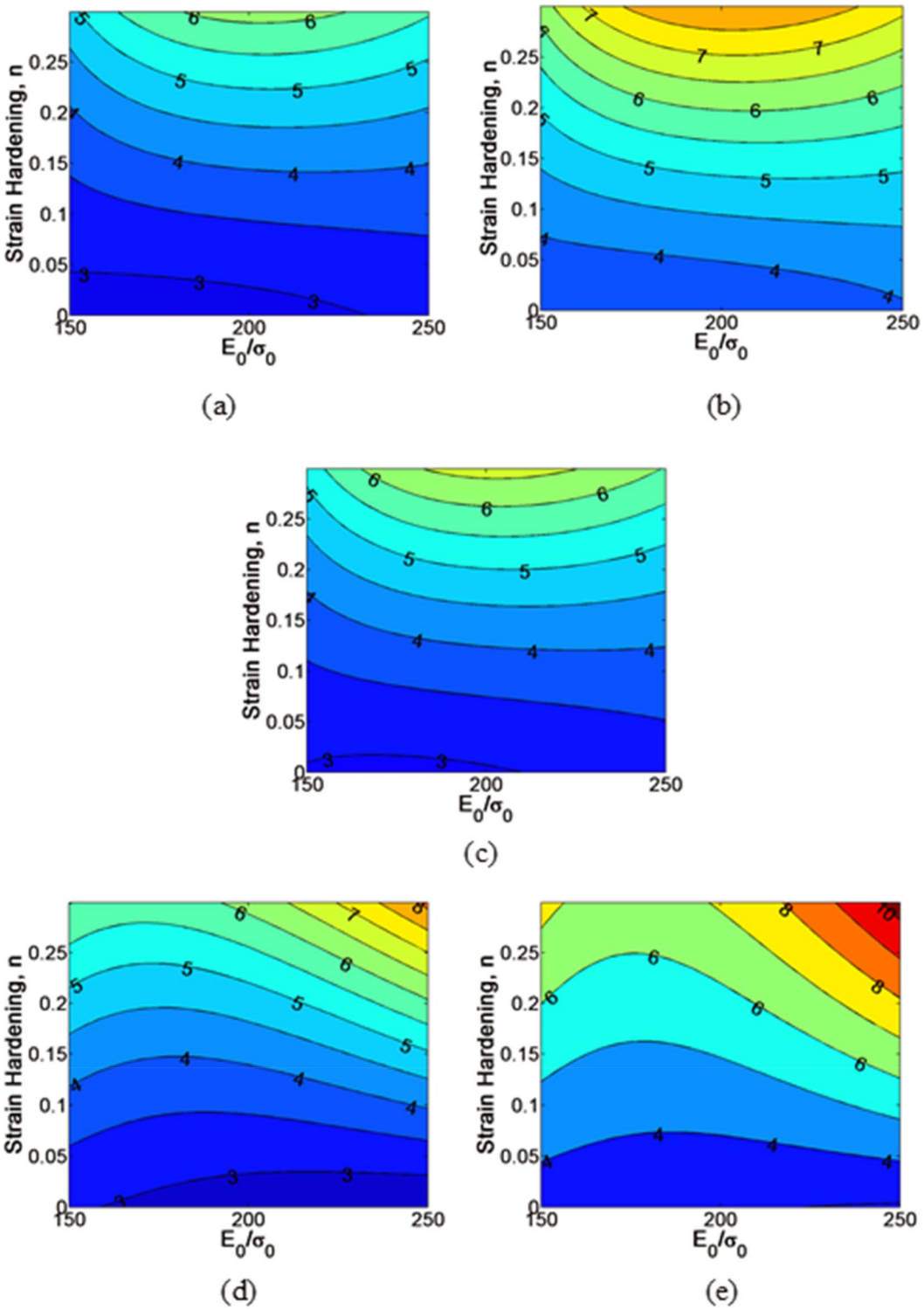

Figure 6: Variation of the ratio of hardness to average yield stress σ_0, with varying strain hardening and E_0/σ_0 for: (a) materials with elastic anisotropy indented in the longitudinal direction; (b) materials with plastic anisotropy indented in the longitudinal direction; (c) isotropic materials; (d) materials with elastic anisotropy indented in the transverse direction; and (e) materials with plastic anisotropy indented in the transverse direction.

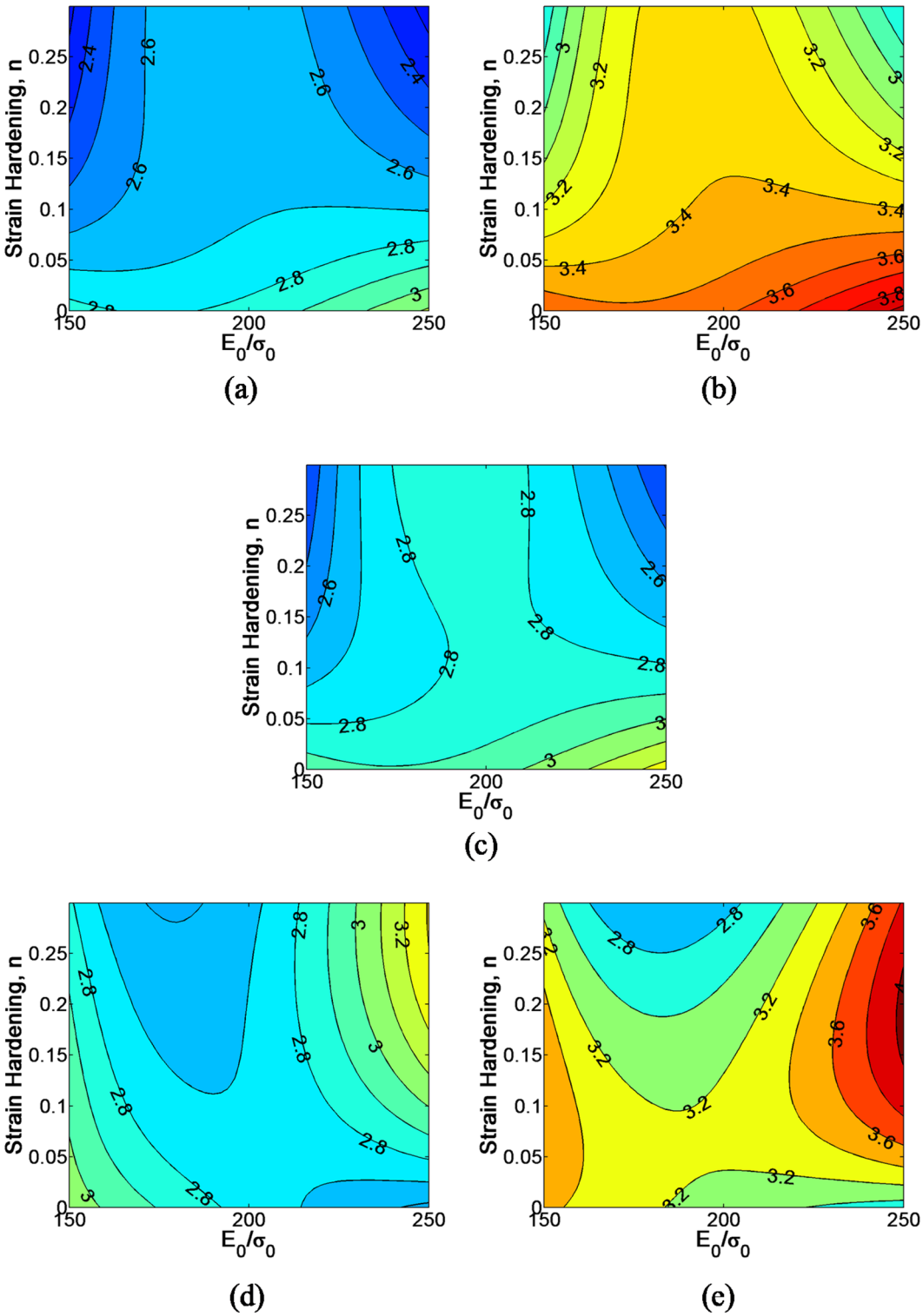

Figure 7: Variation of the ratio of hardness to the average Tabor's representative stress with varying strain hardening and E_0/σ_0 for (a) materials with elastic anisotropy indented in the longitudinal direction; (b) materials with plastic anisotropy indented in the longitudinal direction; (c) isotropic materials; (d) materials with elastic anisotropy indented in the transverse direction; and (e) materials with plastic anisotropy indented in the transverse direction.

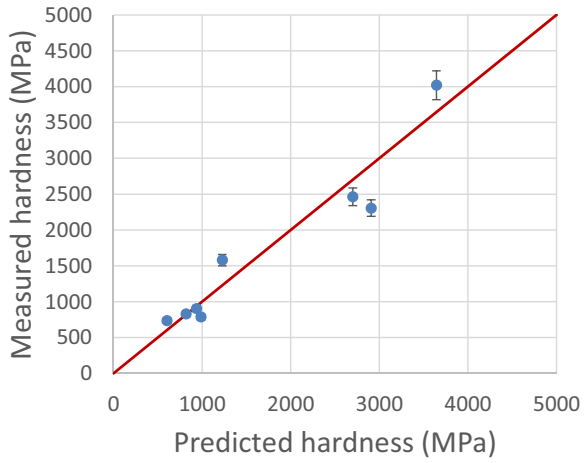

Figure 8: Comparison of hardness predicted by the model developed in this study with experimentally measured hardness for several transversely isotropic materials.

lus, the average yield stress, and the strain-hardening exponent. However, multiple materials with different combinations of elastic and plastic properties may exhibit identical hardness values.

(iii) The hardness of a transversely isotropic material is higher when it exhibits a certain level of plastic anisotropy when compared to a material which exhibits the same level of elastic anisotropy, when both these materials have the same average elastic modulus and yield strengths.

(iv) When compared to materials that have low strain-hardening characteristics, the hardness of materials that have higher strain-hardening exhibits a greater level of sensitivity to the anisotropy in the elastic and plastic properties.

(v) For materials with no strain hardening, the ratio of the hardness to average yield stress (R_0) can vary from 2.5 to 3.5 depending on the materials' average elastic and plastic properties and degree of anisotropy. However, for materials with strain hardening, R_0 can be as high as 10.

(vi) The ratio of the hardness to the Tabor's representative stress (R_t) can vary between 2.2 and 4, depending on the materials' average elastic and plastic properties and the degree of anisotropy.

(vii) The hardness predicted for a range of real-life transversely isotropic materials compare well with the experimentally determined values obtained from the literature.

Methods

In the present study, a combination of dimensional analysis and finite element simulations is invoked to develop a framework that establishes the relationships between the elastic and plastic properties of transversely isotropic materials and their indentation hardness along the longitudinal and transverse directions.

Dimensional analysis

For a sharp indenter with a half cone angle of θ, the load – P, required to indent a power-law hardening transversely isotropic material can be written as follows:

$$P = P\left(h, E_0, \sigma, \frac{E_L}{E_T}, \frac{\sigma_L}{\sigma_T}, n, \theta\right). \tag{8}$$

Using dimensional analysis Eq. (8) becomes

$$P = \sigma_0 h^2 \Pi_{1\theta}\left(\frac{E_0}{\sigma_0}, \frac{E_L}{E_T}, \frac{\sigma_L}{\sigma_T}, n, \theta\right). \tag{9}$$

The projected area of contact – A_m, can be written as follows:

$$A_m = A_m\left(h, \frac{E_0}{\sigma_0}, \frac{E_L}{E_T}, \frac{\sigma_L}{\sigma_T}, n, \theta\right) \tag{10}$$

and also as

$$A_m = h^2 \Pi_{4\theta}\left(\frac{E_0}{\sigma_0}, \frac{E_L}{E_T}, \frac{\sigma_L}{\sigma_T}, n, \theta\right). \tag{11}$$

Dividing Eqs. 9 by 11 we get a relationship for the indentation hardness—H_m:

$$H_m = \frac{P}{A_m} = \sigma_0 \Pi_5\left(\frac{E_0}{\sigma_0}, \frac{E_L}{E_T}, \frac{\sigma_L}{\sigma_T}, n\right) \tag{12}$$

for a specific θ such as 70.3°.

As the present study considers two indentations, one each along the longitudinal and transverse directions, the corresponding areas of contact and the indentation hardness can be captured as follows:

$$A_m = h^2 \Pi_{4i}\left(\frac{E_0}{\sigma_0}, \frac{E_L}{E_T}, \frac{\sigma_L}{\sigma_T}, n\right); i = 1, 2 \tag{13}$$

$$H_m = \frac{P}{A_m} = \sigma_0 \Pi_{5i}\left(\frac{E_0}{\sigma_0}, \frac{E_L}{E_T}, \frac{\sigma_L}{\sigma_T}, n\right); i = 1, 2, \tag{14}$$

where $i = 1, 2$ represents the direction of indentation, that corresponds, respectively, to longitudinal and transverse indentations.

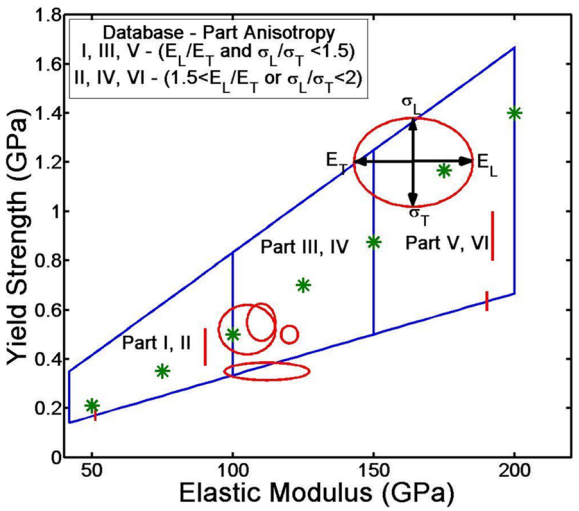

Figure 9: A schematic illustrating the material property database chosen for the present analysis and the division of the database into six domains. Red lines and ellipses indicate the degree of transverse isotropy exhibited by commonly occurring engineering materials. The '*'s indicate the average elastic and plastic properties of some of the transversely isotropic materials chosen for the study.

The actual forms of these dimensionless functions and their formulations are discussed in the next section and summarized in the appendix section.

Computational modeling

Three-dimensional finite element models were developed, in ABAQUS, to simulate the indentation of a large number of transversely isotropic materials which exhibit a wide range of elastic and plastic anisotropy (Fig. 9). A rigid, frictionless conical indenter with a cone half angle of 70.3° was used for the simulations, which has been shown to be equivalent to indentations with a Berkovich indenter (as described in more detail in "Comparison of hardness obtained from Berkovich and equivalent conical indentations" section).

A typical model comprised of 12,000 eight-noded hex-elements with a fine mesh near the contact region and a gradually coarser mesh further away from the contact region to ensure numerical accuracy. The fine inner meshing and the coarser boundary meshing were connected by 30,000 four-noded tetrahedral elements. It was ensured that at the maximum load, the minimum number of contact elements in the contact zone was no less than 225 in each finite element model. The mesh was determined to be insensitive to far-field boundary conditions and was well tested for convergence.

In the present study, 120 materials covering a wide range of possible elastic and plastic behavior were identified. For this purpose, the selected values of the average Young's modulus, E_0, ranged from 50 to 200 GPa, the average yield strength, σ_0, from 210 to 1400 MPa, and the strain-hardening exponent, n, from 0 to 0.3. The Poisson's ratio ν was fixed at 0.3. Also, the ratios of E_L/E_T and σ_L/σ_T were varied from 1 to 2 for each of these cases. This property domain covers a wide range of engineering materials such as steels, aluminum alloys, nickel-based alloys, titanium alloys, thin films, and surface coatings.

The indentation load–depth response characteristics and the area of contact under maximum load for both longitudinal and transverse indentations were obtained in the finite element simulations.

Careful analysis was conducted to determine the exact forms of the dimensionless functions that best described the relationships between the material's elastic and plastic properties, the corresponding indentation response parameters, and the material's hardness. It was found that, in general, no single function was able to accurately capture the relationship between the material properties and the indentation parameters for the whole range of materials that was chosen for the analysis. However, by sub-dividing the whole range of materials into six smaller groups (as indicated in Fig. 9), accurate dimensionless functions were obtained for each group of materials (Appendix A).

For example, the detailed form of one of the dimensionless functions is given as follows:

Table I: A partial list of transversely isotropic engineering materials that exhibit varying degrees of elastic and plastic anisotropy [45–47].

Material	E_0 (GPa)	E_L/E_T	σ_0 (MPa)	σ_L/σ_T	n	ν
Annealed tool steel	192	1	610	1.4	0.1	0.3
Al Castings 242-0T21	71	1	155	1.5	0.16	0.3
Malleable Iron	210	1	285	1.54	0.01	0.3
2124 Al 15% Sic Whiskers	105	1.2	480	1.5	0.1	0.3
Ti-15 V-3Cr-3Al-3Sn	164	1.3	1200	1.35	0	0.4
Zirconium	112	1.3	230	1.4	0.1	0.35
Ductile Iron ASTM A 476–70	210	1	483	1.33	0.1	0.3
Be-Cu Alloy 50C UNS C81800	110	1	238	2	0.18	0.3
Al 6092 17.5 SiC whiskers	121	1.05	452.5	1.15	0.1	0.33
Titanium	123.82	1.37	200	1.57	0.07	0.35

$$\Pi_{154} = \frac{H}{\sigma_0} = \begin{pmatrix} n^2(20.42 + 5.46y^2 - 18.28yz + 6.34z^2)(-229.69 + 87.4Log[x] - 8.25Log[x]^2) + \\ n(1.9 - 5y^2 + 14.46yz - 3.97z^2)(-107.43 + 40.91Log[x] - 3.87Log[x]^2) + \\ (5.42 - 0.12y^2 + 0.14yz + 0.36z^2)(12.42 - 4.6Log[x] + 4.5Log[x]^2) \end{pmatrix} \quad (15)$$

These dimensionless equations are presented as Π_{jkl}, where '*j*' varies from 1 to 2 and signifies the indenter orientation—1 for longitudinal indentation and 2 for transverse indentation; '*k*' varies from 4 to 5 and conveys the type of dimensionless function—4 for A_m and 5 for H_m; and '*l*' represents the material group number and varies from 1 to 6. x, y, and z represent the properties E_0, E_L/E_T, and σ_L/σ_T, respectively, and *n* represents the strain-hardening exponent.

For those materials which are at the boundary of any two material groups (i.e., materials common to two regions), the dimensionless function that correspond to the lower region (i.e., region with the lower designation) is consistently used for the analysis in this study. For example, for materials common to both regions I and II (Fig. 9), the dimensionless functions pertaining to region I are used for the forward analysis (for predicting indentation responses from material properties). It has been verified that, for both isotropic and transversely isotropic materials on the boundaries (e.g., between region I and II), the differences in the values of the dimensionless functions corresponding to the adjacent regions (i.e., regions I and II) are no more than 5%, thus ensuring good accuracy in the reverse analysis (for obtaining material properties from indentation responses) as well.

Funding

The present study was supported in part by a National Science Foundation Grant DMR-2004944.

Data availability

The raw data required to reproduce these findings are available upon request.

Code availability

N/A.

Declarations

Conflict of interest The authors declare that they have no known competing financial interests or personal relationships that could have appeared to influence the work reported in this paper.

Appendix A

As described in "Computational modeling" section, the entire material property database was divided into six domains. For each of the material domains, dimensionless functions that capture the relationships between true projected contact area (A_m), the indentation hardness (H_m) and the five elastic and plastic properties of transversely isotropic materials (E_0, σ_0, E_L/E_T, σ_L/σ_T, n) are identified. Here, of the 24 equations, a list of 6 dimensionless functions for longitudinal indentation hardness is provided. The equations are listed as Π_{jkl}. Here, j varies from 1 to 2 and signifies the indenter orientation—1 for longitudinal, and 2 for parallel indentation; k varies from 4 to 5, and conveys the type of dimensionless function—4 for A_m and 5 for H_m; and l represents the part number and varies from 1 to 6. X, Y, and Z represent the properties E_0, E_L/E_T, and σ_L/σ_T, respectively.

$$\Pi_{151} = \frac{H}{\sigma_0} = \begin{pmatrix} n^2(17.92 - 3.7y^2 + 0.2yz - 2.1z^2)(241.1 - 92.88Log[x] + 9.01Log[x]^2) + \\ n(-0.13 - 0.66y^2 + 6.18yz - 0.07z^2)(-35.98 + 13.65Log[x] - 1.26Log[x]^2) + \\ (2.6 - 0.13y^2 + 0.17yz + 0.17z^2)(16 - 5.68Log[x] + 0.54Log[x]^2) + \end{pmatrix} \quad (A.1)$$

$$\Pi_{152} = \frac{H}{\sigma_0} = \begin{pmatrix} n^2(39.6 + 13y^2 - 34yz + 17.85z^2)(255.37 - 95.3Log[x] + 8.9Log[x]^2) + \\ n(-9 + 4.27y^2 - 9.79yz + 3.47z^2)(263.75 - 98Log[x] + 9.1Log[x]^2) + \\ (3.6 - 0.09y^2 + 0.13yz + 0.24z^2)(11.9 - 4.17Log[x] + 0.4Log[x]^2) \end{pmatrix} \quad (A.2)$$

$$\Pi_{153} = \frac{H}{\sigma_0} = \begin{pmatrix} n^2(21.5 + 16.3y - 41.7yz + 19.15z^2)(-334.5 + 127.6Log[x] - 12.13Log[x]^2) \\ +n(1.2 - 7.6y^2 + 19.1yz - 7.27z^2)(65.3 - 25.3Log[x] + 2.5Log[x]^2) + \\ (1.85 + 0.02y^2 - 0.11yz + 0.23z^2)(12.8 - 4.5Log[x] + 0.45Log[x]^2) \end{pmatrix} \quad (A.3)$$

$$\Pi_{154} = \frac{H}{\sigma_0} = \begin{pmatrix} n^2(20.4 + 5.46y^2 - 18.28yz + 6.34z^2)(-229.7 + 87.4Log[x] - 8.25Log[x]^2) \\ +n(1.9 - 4.97y^2 + 14.46yz - 3.97z^2)(-107.4 + 40.9Log[x] - 3.9Log[x]^2) \\ +(5.4 - 0.12y^2 + 0.14yz + 0.36z^2)(12.42 - 4.6Log[x] + 0.45Log[x]^2) \end{pmatrix} \quad (A.4)$$

$$\Pi_{155} = \frac{H}{\sigma_0} = \begin{pmatrix} n^2(494.4 - 37y^2 + 90.58yz - 13.6z^2)(-40.54 + 15.9Log[x] - 1.56Log[x]^2) \\ +n(117.7 - 9.45y^2 + 24.6yz + 9.04z^2)(42.1 - 16.54Log[x] + 1.63Log[x]^2) \\ +(5 - 0.52y^2 + 0.94yz + 0.28z^2)(19.1 - 7.42Log[x] + 0.74Log[x]^2) \end{pmatrix} \quad (A.5)$$

$$\Pi_{156} = \frac{H}{\sigma_0} = \begin{pmatrix} n^2(208.26 - 11.76y^2 + 20.3yz + 2.9z^2)(-143.3 + 56.35Log[x] - 5.5Log[x]^2) \\ +n(172.35 - 11.64y^2 + 19.7yz + 4.7z^2)(40.5 - 15.9Log[x] + 1.56Log[x]^2) \\ +(11 - 0.72y^2 + 1.28yz + 0.5z^2)(20.4 - 8Log[x] + 0.8Log[x]^2) \end{pmatrix} \quad (A.6)$$

Supplementary Information

The online version contains supplementary material available at https://doi.org/10.1557/s43578-022-00730-y.

References

1. B. Backes, K. Durst, M. Goken, Determination of plastic properties of polycrystalline metallic materials by nanoindentation: Experiments and finite element simulations. Philos. Mag. **86**, 5541–5551 (2006)
2. Y.W. Bao, W. Wang, Y.C. Zhou, Investigation of the relationship between elastic modulus and hardness based on depth-sensing indentation measurements. Acta Mater. **52**, 5397–5404 (2004)
3. J.L. Bucaille, S. Stauss, E. Felder, J. Michler, Determination of plastic properties of metals by instrumented indentation using different sharp indenters. Acta Mater. **51**, 1663–1678 (2003)
4. J.L. Bucaille, S. Stauss, P. Schwaller, J. Michler, A new technique to determine the elastoplastic properties of thin metallic films using sharp indenter. Thin Solid Films **447**, 239–245 (2004)
5. K.S. Chen, T.C. Chen, K.S. Ou, Development of semi-empirical formulation for extracting materials properties from nanoindentation measurements: Residual stresses, substrate effect, and creep. Thin Solid Films **516**, 1931–1940 (2008)
6. W.M. Chen, M. Li, T. Zhang, Y.T. Chen, C.M. Cheng, Influence of indenter tip roundness on hardness behavior in nanoindentation. Mater. Sci. Eng. A Struct. **445**, 323–327 (2007)
7. Y.T. Cheng, C.M. Cheng, Scaling, dimensional analysis, and indentation measurements. Mater. Sci. Eng. R. **44**, 91–149 (2004)
8. N. Chollacoop, M. Dao, S. Suresh, Depth-sensing instrumented indentation with dual sharp indenters. Acta Mater. **51**, 3713–3729 (2003)
9. M. Tian, T.A. Venkatesh, Indentation of shape memory polymers: Characterization of thermomechanical and shape memory properties. Polymer **54**, 1405–1414 (2013)
10. G. Cheng, T.A. Venkatesh, Dominant factors influencing the nanoindentation response of piezoelectric materials: A case study in relaxor ferroelectrics. Philos. Mag. Lett. **93**, 116–128 (2013)
11. A.E. Giannakopoulos, P.L. Larsson, R. Vestergaard, Analysis of Vickers indentation. Int. J. Solids Struct. **31**, 2679–2708 (1994)
12. K. Kese, Z.C. Li, Semi-ellipse method for accounting for the pile-up contact area during nanoindentation with the Berkovich indenter. Scr. Mater. **55**, 699–702 (2006)
13. H. Lan, T.A. Venkatesh, On the uniqueness and sensitivity issues in determining the elastic and plastic properties of power-law hardening materials through sharp and spherical indentation. Philos. Mag. **87**, 4671–4729 (2007)
14. H. Lan, T.A. Venkatesh, On the sensitivity characteristics in the determination of the elastic and plastic properties of materials through multiple indentation. J. Mater. Res. **22**, 1043–1063 (2007)
15. H. Lan, T.A. Venkatesh, Determination of the elastic and plastic properties of materials through instrumented indentation with reduced sensitivity. Acta Mater. **55**, 2025–2041 (2007)
16. P.L. Larsson, On the mechanical behavior of global parameters in the material characterization by sharp indentation testing. J. Test Eval. **32**, 310–321 (2004)
17. P.L. Larsson, A.E. Giannakopoulos, E. Soderlund, D.J. Rowcliffe, R. Vestergaard, Analysis of Berkovich indentation. Int. J. Solids Struct. **33**, 221–248 (1996)
18. J.H. Lee, H. Lee, D.H. Kim, A numerical approach to evaluation of elastic modulus using conical indenter with finite tip radius. J. Mater. Res. **23**, 2528–2537 (2008)

19. M. Lichinchi, C. Lenardi, J. Haupt, R. Vitali, Simulation of Berkovich nanoindentation experiments on thin films using finite element method. Thin Solids Films. **333**, 278–286 (1998)
20. Y.Y. Lim, M.M. Chaudhri, The effect of the indenter load on the nanohardness of ductile metals: An experimental study on polycrystalline work-hardened and annealed oxygen-free copper. Philos. Mag. A. **79**, 2979–3000 (1999)
21. M. Dao, N. Challocoop, K.J. Van Vliet, T.A. Venkatesh, S. Suresh, Computational modeling of forward and reverse problems in instrumented sharp indentation. Acta Mater. **49**, 3899–3918 (2001)
22. N. Ogasawara, N. Chiba, X. Chen, Measuring the plastic properties of bulk materials by single indentation test. Scr. Mater. **54**, 65–70 (2006)
23. W.C. Oliver, Alternative technique for analyzing instrumented indentation data. J. Mater. Res. **16**, 3202–3206 (2001)
24. W.C. Oliver, G.M. Pharr, An improved technique for determining hardness and elastic modulus using load and displacement sensing indentation experiments. J. Mater. Res. **7**, 1564–1583 (1992)
25. W.C. Oliver, G.M. Pharr, Nanoindentation in materials research: Past, present, and future. MRS Bull. **35**, 897–907 (2010)
26. G.M. Pharr, A. Bolshakov, Understanding nanoindentation unloading curves. J. Mater. Res. **17**, 2660–2671 (2002)
27. T.A. Venkatesh, K.J. Van Vliet, A.E. Giannakopoulos, S. Suresh, Determination of elasto-plastic properties by instrumented sharp indentation: Guidelines for property extraction. Scr. Mater. **42**, 833–839 (2000)
28. J.T. Wang, P.D. Hodgson, C.H. Yang, Effects of mechanical properties on the contact profile in Berkovich nanoindentation of elastoplastic materials. J. Mater. Res. **27**, 313–319 (2012)
29. Z.H. Xu, D. Rowcliffe, Method to determine the plastic properties of bulk materials by nanoindentation. Philos. Mag. A. **82**, 1893–1901 (2002)
30. H. Lan, T.A. Venkatesh, On the relationships between hardness and the elastic and the plastic properties of isotropic power-law hardening materials. Philos. Mag. A. **93**, 35–55 (2014)
31. X.Z. Xiao, L. Yu, Nano-indentation of ion-irradiated nuclear structural materials: A review. Nuclear Mater. Energy **22**, 100721 (2020)
32. M.M. Chaudhri, Indentation hardness of diamond single crystals, nanopolycrystal, and nanotwinned diamonds: A critical review. Diamond Mater. **109**, 108076 (2020)
33. M.M. Islam, S.I. Shaki, N.M. Shaheen, P. Bayati, M. Haghshenas, An overview of microscale indentation fatigue: Composites, thin films, coatings, and ceramics. Micron **148**, 103110 (2021)
34. A. Gouldstone, N. Chollacoop, M. Dao, J. Li, A.M. Minor, Y.-L. Shen, Indentation across size scales and disciplinesrecent developments in experimentation and modeling. Acta Mater. **55**, 4015–4039 (2007)
35. T. Rouxel, J.I. Jang, U. Ramamurty, Prog. Mater. Sci. **121**, 1 (2021)
36. A.C. Fischer-Cripps, S.J. Bull, N. Schwarzer, Critical review of claims for ultra-hardness in nanocomposite coatings. Philos. Mag. **92**(1601), 1630 (2012)
37. C.A. Schuh, Nanoindentation studies of materials. Mater. Today **9**, 32–40 (2006)
38. Q. Wang, F. Long, Z. Wang, N. Guo, M.R. Daymond, Orientation dependent evolution of plasticity of irradiated Zr-25.Nb pressure tube alloy studied by nanoindentation and finite element modeling. J. Nucl. Mater. **512**, 371–384 (2018)
39. S.M. Kalkhoran, W.B. Choi, A. Gouldstone, Estimation of plastic anisotropy in Ni–5% Al coatings via spherical indentation. Acta Mater. **60**, 803–810 (2012)
40. G. Cheng, X. Sun, Y. Wang, S.L. Tay, W. Gao, Nanoindentation study of electrodeposited Ag thin coating: An inverse calculation of anisotropic elastic-plastic properties. Surf. Coat. Technol. **310**, 43–50 (2017)
41. A. Yonezu, K. Yoneda, H. Hirakata, M. Sakihara, K. Minoshima, A simple method to evaluate anisotropic plastic properties based on dimensionless function of single spherical indentation-application to SiC whisker-reinforced aluminum alloy. Mater. Sci. Eng. A **527**, 7646–7657 (2010)
42. Z. Fan, J.Y. Rho, Three-dimensional finite element analysis of the effects of anisotropy on bone mechanical properties measured by nanoindentation. J. Mater. Res. **19**, 114–123 (2004)
43. Z.J. Cheng, X.M. Wang, J. Ge, J.X. Yan, N. Ji, L.L. Tian, F.Z. Cui, The mechanical anisotropy on a longitudinal section of human enamel studied by nanoindentation. J. Mater. Sci.: Mater. Med. **21**, 1811–1816 (2010)
44. A. Jäger, Th. Bader, K. Hofstetter, J. Eberhardsteiner, The relation between indentation modulus, microfibril angle, and elastic properties of wood cell walls. Compos. A **42**, 677–685 (2011)
45. T.S. Bhat, T.A. Venkatesh, Indentation of transversely isotropic power-law hardening materials: Computational modelling of the forward and reverse problems. Philos. Mag. A. **93**, 4488–4518 (2013)
46. ASM Handbook: Properties and Selection Vol. I, II ASM International, Materials Park, OH (1990).
47. ASM.Matweb.com
48. J.J. Vlassak, M. Ciavarella, J.R. Barber, X. Wang, The indentation modulus of elastically anisotropic materials for indenters of arbitrary shape. J. Mech. Phys. Sol. **51**, 1701–1721 (2003)
49. Y.F. Gao, G.M. Pharr, Multidimensional contact moduli of elastically anisotropic solids. Scr. Mater. **57**, 13–16 (2007)
50. C. Jin, Numerical investigation of indentation tests on a transversely isotropic elastic material by power-law shaped axisymmetric indenters. J. Adhesion. Sci. Tech. **30**, 1223–1242 (2016)
51. F.M. Borodich, B.A. Galanov, L.M. Keer, M.M. Suarez-Alvarez, The JKR-type adhesive contact problems for transversely isotropic elastic solids. Mech. Mater. **75**, 34–44 (2014)

52. T.L. Li, J.H. Lee, Y.F. Gao, An approximate formulation of the effective indentation modulus of elastically anisotropic film-on-substrate systems. Int. J. Appl. Mech. **1**, 515–525 (2009)
53. M. Wang, J. Wu, X. Zhan, R. Guo, Y. Hui, H. Fan, On the determination of the anisotropic plasticity of metal materials by using instrumented indentation. Mater. Des. **111**, 98–107 (2016)
54. J. Wu, M. Wang, Y. Hui, Z. Zhang, H. Fan, Identification of anisotropic plasticity properties of materials using spherical indentation imprint mapping. Mater. Sci. Eng. A **723**, 269–278 (2018)
55. T. Nakamura, Y. Gu, Identification of elastic-plastic anisotropic parameters using instrumented indentation and inverse analysis. Mech. Mater. **39**, 340–356 (2007)
56. A. Yonezu, M. Tanaka, R. Kusano, X. Chen, Probing out-of-plane anisotropic plasticity using spherical indentation: A numerical approach. Comput. Mater. Sci. **79**, 336–344 (2013)
57. D. Tabor, An improved equation relating hardness to ultimate strength. J. I Met. **79**, 1–18 (1951)